Long-Term Monitoring of Cropland Change near Dongting Lake, China, Using the LandTrendr Algorithm with Landsat Imagery

Lihong Zhu, Xiangnan Liu *, Ling Wu, Yibo Tang and Yuanyuan Meng

School of Information Engineering, China University of Geosciences, Beijing 100083, China;
zhulh@cugb.edu.cn (L.Z.); wuling@cugb.edu.cn (L.W.); delicktang@cugb.edu.cn (Y.T.);
mengyy@cugb.edu.cn (Y.M.)
* Correspondence: liuxn@cugb.edu.cn; Tel.: +86-10-8232-3056

check for
updates

Abstract: Tracking cropland change and its spatiotemporal characteristics can provide a scientific basis for assessments of ecological restoration in reclamation areas. In 1998, an ecological restoration project (Converting Farmland to Lake) was launched in Dongting Lake, China, in which original lake areas reclaimed for cropland were converted back to lake or to poplar cultivation areas. This study characterized the resulting long-term (1998–2018) change patterns using the LandTrendr algorithm with Landsat time-series data derived from the Google Earth Engine (GEE). Of the total cropland affected, ~447.48 km^2 was converted to lake and 499.9 km^2 was converted to poplar cultivation, with overall accuracies of 87.0% and 83.8%, respectively. The former covered a wider range, mainly distributed in the area surrounding Datong Lake, while the latter was more clustered in North and West Dongting Lake. Our methods based on GEE captured cropland change information efficiently, providing data (raster maps, yearly data, and change attributes) that can assist researchers and managers in gaining a better understanding of environmental influences related to the ongoing conversion efforts in this region.

Keywords: cropland change patterns; LandTrendr algorithm; Landsat time series; Google Earth Engine; Dongting Lake; China

1. Introduction

Dongting Lake, once the largest freshwater lake in China, has shrunk to the second-largest due to land reclamation for agriculture; this has resulted in serious ecological degradation of the area's wetlands [1]. After the devastating flood in 1998, the government promoted the project of Converting Farmland to Lake (CFTL) and planned to abandon 785.7 km^2 of cropland area, where conversion to lake or poplar trees cultivation could establish a new balance between economic benefits and the regulation of wetland ecological functions. These efforts have created a need for long-term monitoring of cropland change processes to provide scientific data for ongoing ecological management after project completion.

Although field surveys are the most accurate monitoring method for this purpose, they are impractical over large areas due to time constraints and the inability to assess certain inaccessible sites (such as shoal areas). In contrast, remote sensing techniques enable frequent imaging, easier access, and larger-scale monitoring, becoming important global data sources for detecting environmental changes (including those to cropland) [2–4]. The moderate resolution of publicly available USGS Landsat data [5] makes them suitable for monitoring changes in agriculture fields [6–8]. Detection of cropland change can be based on comparisons between two or more Landsat images [9–11], and to

date, many studies have applied Landsat time-series analysis to long-term monitoring of cropland change [12,13]. Such remote sensing time series can be used to separate long-term and short-term land-use changes more reliably in highly resilient land systems. Zhe [14] provided a comprehensive review of change detection approaches using Landsat time-series data, including the description of frequencies, preprocessing, algorithms, and applications.

Choosing a suitable algorithm is a critical step for conducting change detection [15]. Several change-detection techniques based on Landsat time series have been developed to be robust against spectral variations arising from topography and phenology [16]. For example, Landsat-based Detection of Trends in Disturbance and Recovery (LandTrendr) and Breaks For Additive Season and Trend (BFAST) have been applied to monitor cropland change [17,18]. BFAST has been used to investigate cropping systems and temporal paddy crop dynamics in Sidoarjo Regency, Indonesia, and provide accurate and up-to-date information on agricultural land-use changes [19,20]. LandTrendr can be used to identify cropland abandonment and re-cultivation based on annual time series of cropland probabilities; it can also contribute to the identification of different smallholder cultivation patterns [21,22].

The above change-detection algorithms, and others such as Continuous Change Detection and Classification (CCDC) [23] are subject to considerable computational time in data-preprocessing and are themselves time-consuming. In order to reach to a broader research community, the LandTrendr algorithm (https://emapr.github.io/LT-GEE/) was implemented on the Google Earth Engine (GEE) platform, which provides full access to the Landsat archive and parallel processing to increase computational speed [24]. Compared to previous change detection algorithms run on local servers [25,26], LandTrendr in GEE detects cropland change more efficiently with the advantages of cloud computing and offers an opportunity to map large-scale cropland change [27].

Previous change assessment studies have focused on cropland abandonment and re-cultivation and detecting changes in their cultivation patterns. Thus, cropland conversion to other land cover classes in areas such as Dongting Lake in China has not received much attention. Using LandTrendr with GEE support, we can observe the process of cropland conversion to lake or poplar trees and its spatial and temporal characteristics efficiently, understanding this process can provide the policy enlightenment for ecological conservation in Dongting Lake.

Our overarching goal therefore was to use LandTrendr with Landsat time-series in GEE to detect cropland change processes in the Dongting Lake area, we analyzed a conceptual model of the spectral feature trajectories related to cropland conversion to lake or poplar cultivation. We also parameterized the LandTrendr algorithm and tested it based on Landsat time-series data to track these changes, then compared their spatial and temporal characteristics.

2. Materials and Methods

2.1. Study Area

Dongting Lake (28°42′–29°38′ N, 111°52′–113°08′ E), located in the north part of Hunan Province, is the second largest freshwater lake in China with an area of 2794.7 km² [28]. We defined our study area by administrative divisions in the lake's surrounding area, including 20 counties (districts) in Yueyang, Yiyang, and Changde (Figure 1). This area included reclamation zones outside the Dongting Lake embankment with internal lakes used mainly for agricultural production; while the area within the embankment included the outer lake (East Dongting Lake, South Dongting Lake, Hengling Lake, and West Dongting Lake).

There has been excessive reclamation of the lake for almost 100 years, resulting in serious ecological degradation of the wetland ecosystem associated with the lake. Following the great Yangtze River flood in 1998, the CFTL was launched to help restore the lake's ecology and guide the area's development in a more benign direction. After the project was initiated, agricultural land focused on two change patterns: conversions back to lake were implemented mainly around in the outer lake area to improve

ecological functions, while poplar trees cultivation was implemented primarily in part of the outer lake for economic benefits.
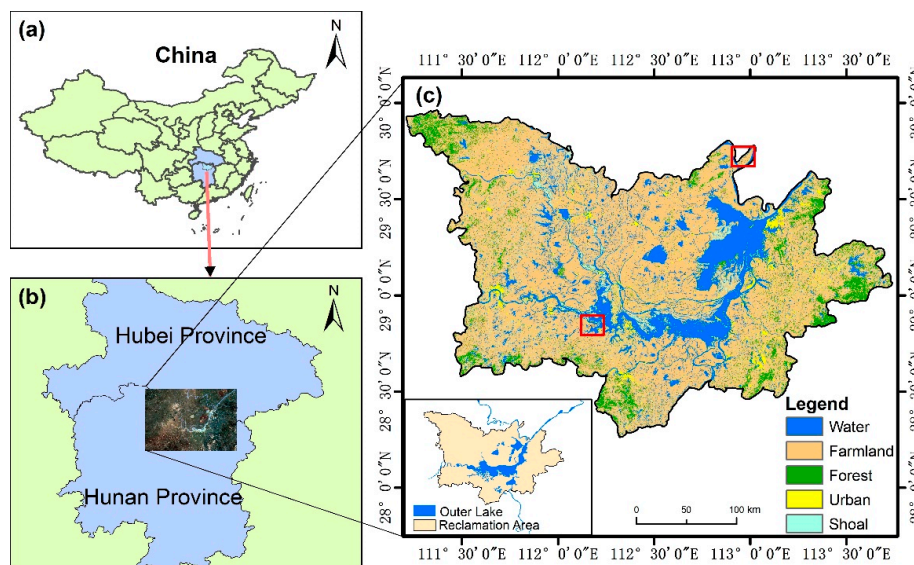
Figure 1. Geographic location and land cover map of the study area: (**a**) general location in China; (**b**) location in Hunan Province; (**c**) 1997 land-use classification (prior to Converting Farmland to Lake (CFTL) implementation) from Google Earth Engine (GEE) imagery (see Section 2.3). The red frames show the location of the two typical CFTL areas.

Two typical CFTL areas (Figure 1), the Qingshan Polder (28°51′ N, 112°12′ E) with an area of 11.1 km^2 and the Jicheng polder (29°41′ N, 112°56′ E) with an area of 33.7 km^2, are taken as examples (Figure 2). The local government led its cropland conversion to natural lake after 1998 with Qingshan Polder, aiming to restore a wetland ecosystem. As a typical demonstration area for the CFTL project, Qingshan developed a green aquatic culture that did not require fertilizer or feed for recovery. At Jicheng Polder, many poplars were planted to form a plantation forest system, based on the pattern of poplar cultivation after local residents moved outside the village and abandoned the cropland. Poplar cultivation can alleviate the tight supply of medicinal materials and promote the development of a local economy [29].
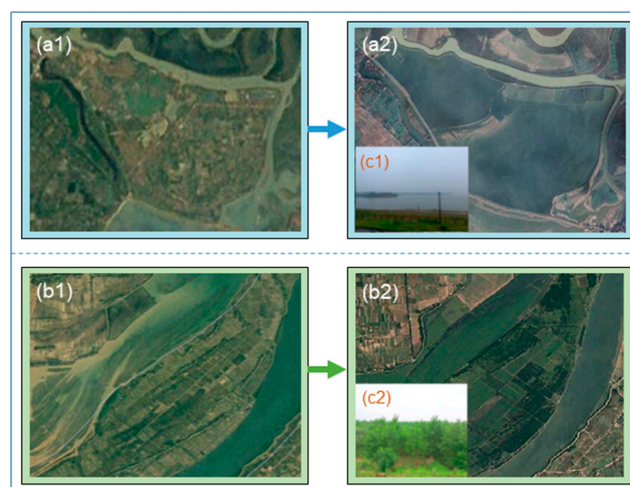
Figure 2. Two examples areas of each cropland change pattern. Corresponding photos a1 and a2, b1 and b2 before and after CFTL are from google earth to demonstrate the process of conversion to lake, poplar cultivation respectively. Figures a1 and b1 represent the years 1997 and figures a2 and b2 the years 2018. Field photographs c1 and c2 were collected in 2018.

2.2. Data Preparation

We used the GEE platform's full archive to build stacks of Surface Reflectance Tier 1 Landsat TM/ETM+/OLI images from 1998–2018 for use with LandTrendr (Table 1). In order to minimize variations caused by phenology or changes in solar geometry, a total of 320 images across three path/row numbers were acquired in the crop-growing season (June 1 to September 1) within the whole study period. As the Landsat 8/OLI has higher 12-bit radiometric resolution than the previous Landsat 7/ETM+, we applied statistical harmonization functions between the spectral values of both sensors to normalize the reflectance [30]. Cloud, cloud shadow, and snow masks were produced from the Fmask band. Finally, 21 annual composites from 320 images with minimal cloud cover were created using the median reflectance values of the collection [31].

Table 1. Datasets used in this study.

| Data	Description	Source
Landsat5 Landsat7 Landsat8 (path/row: 123/040,124/039,124/040)	Annual atmospherically corrected Surface Reflectance Collection from June to September, 1998–2018, for use with LandTrendr	Pre-Collection 1 archive available from Google Earth Engine
DEM	Advanced Spaceborne Thermal Emission and Reflection Radiometer (ASTER) data used for modification of classification	ASTER Global Emissivity Dataset 100 m V003 available from Google Earth Engine
Field survey	Inventory data within the study area, collected in 2018	
High-resolution images	Imagery used for validation of LandTrendr disturbance	Google Earth

2.3. Cropland Change Conceptual Model

Figure 3 presents the conceptual model of two cropland change patterns, from which the pattern of conversion to either lake cover over poplar cultivation can be seen; this results in a mixed pattern of changes. To focus on the pattern of conversions to lakes, we removed poplar cultivations by subtracting the superposition results of the two patterns using ArcGIS 10.4. Normalized Difference Vegetation Index (NDVI) is a useful indicator for monitoring vegetation changes in agricultural change areas [32,33], so we used this to detect cropland changes in this study. We captured as many examples of cropland conversion as possible to know how NDVI signatures would represent the cropland conversions. When cropland is converted to lake, the initially higher NDVI should drop to a much lower level (Figure 3a). When cropland is converted to poplar cultivation, NDVI should drop temporarily but recover to a higher level than before (Figure 3b). These proposed trajectories reflect occurrence, duration, and magnitude attributes, which respectively express the year of occurrence, duration time, and the range of NDVI variation during conversion.
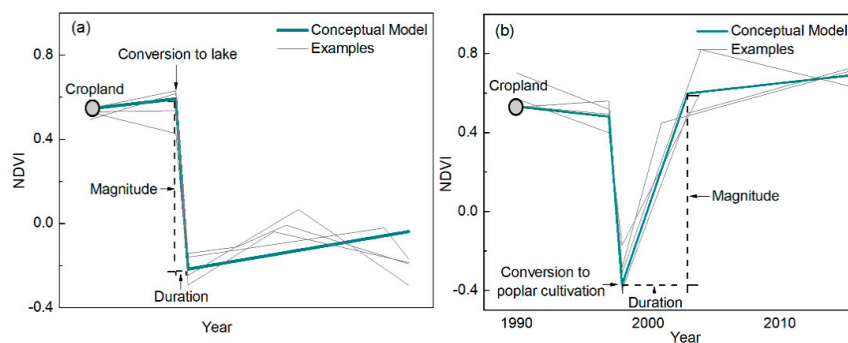
Figure 3. Conceptual models and several examples for cropland conversion in the CFTL: (**a**) Normalized Difference Vegetation Index (NDVI) trajectory of conversion to lake; (**b**) NDVI trajectory of conversion to poplar cultivation.

2.4. Initial Land Cover Classification

Prior to running the LandTrendr algorithm, we applied the Random Forest (RF) classifier [34] to pre-CFTL Landsat images in GEE to extract cropland areas (Figure 4a). First, Landsat images from 1997 were used with the cloud and shadow masks to produce a cloud-free composite, from which the NDVI was calculated. Next, 250 training samples for each land-cover class were selected for interpretation by high-resolution imagery from Google Earth. As NDVI can be used to distinguish impervious surfaces, bare soil, and water bodies from forest or croplands, this along with bands one through five, and seven were used as feature inputs into the RF classifier with 20 trees. The resulting imagery was classified into five land-cover categories: water, cropland, forest, urban, and shoal. Finally, elevation and slope derived from GEE DEM data were used to modify the classification results for higher accuracy. In 1997, the major land cover types were cropland and water (Figure 1c).
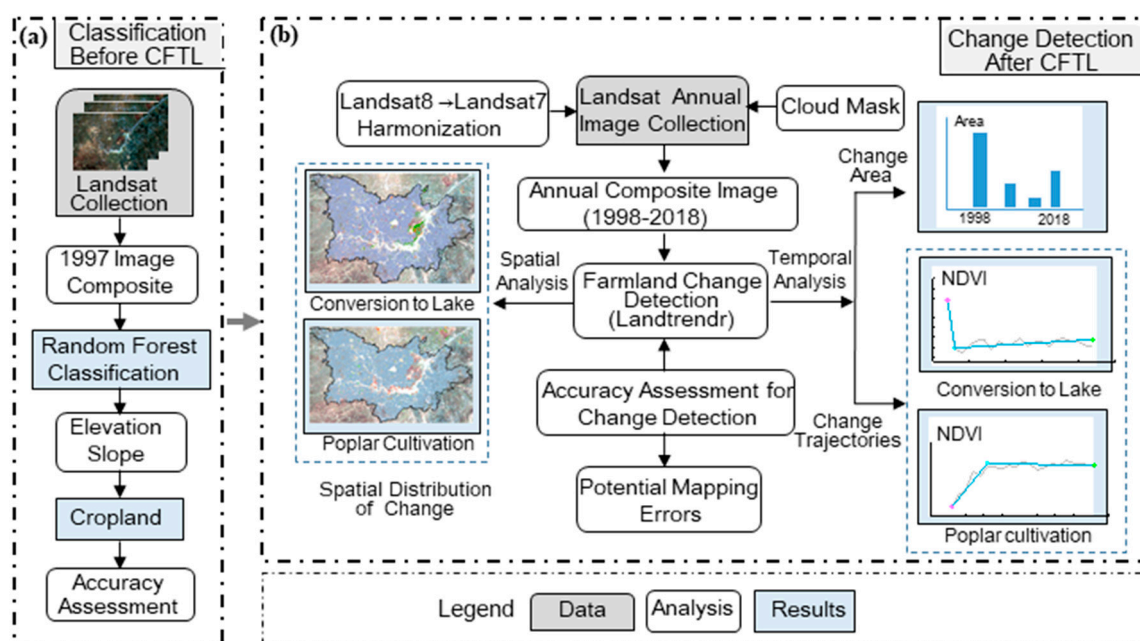

Figure 4. Methodological flowchart for (**a**) pre-CFTL land-use classification and (**b**) post-CFTL analysis of conversion to lake and poplar cultivation.

2.5. Monitoring Cropland Change with LandTrendr

We used the LandTrendr algorithm developed by Kennedy [35] to map and characterize post-CFTL cropland changes (Figure 4b). The core of the LandTrendr algorithm is a temporal segmentation method used to capture both long-term gradual and short-term drastic changes; this approach can monitor cropland change by analyzing the temporal-spectral trajectory of each pixel. The input for each pixel is the annual time series of one spectral band or index, plus the date. The processing procedure for finding the best model involves removing noise-induced spikes (outliers), identifying potential vertices (breakpoints), fitting trajectories, and setting the optimal number of segments [23].

LandTrendr requires the setting of control parameters to ensure the quality of change detection, so we analyzed examples of cropland conversion event, tested different combinations of parameter values to determine the optimal combination of parameters. We also assessed the characteristics of NDVI in the study area to exclude other change patterns in order to make LandTrendr more precise (Figure 5). NDVI before conversion ranged from 0.55–0.73, dropped sharply after conversion to lake (–0.25 to –0.16), and rose slightly after conversion to poplar cultivation (0.57–0.77). Therefore, for the event of conversion to lake, we set the pre-lake-conversion NDVI to be >0.55 and the magnitude of NDVI decrease should be >0.71. While for the event of poplar cultivation, the pre-poplar-cultivation NDVI > –0.25 and the magnitude of NDVI increase should be >0.73.
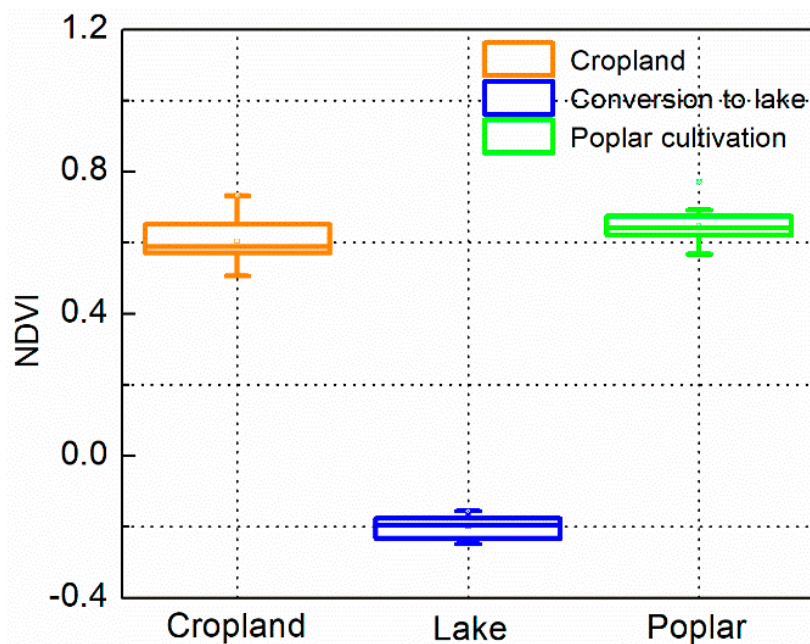
Figure 5. NDVI range of cropland, conversion to lake, and conversion to poplar cultivation in the study area.

2.6. Accuracy Assessment and Validation

To assess the accuracy of the 1997 classification results, we selected validation sites different from those used for training the classification algorithm, randomly generating 180 samples for each land-cover class. We then produced a confusion matrix and estimates of overall accuracy, user accuracy, and producer accuracy for each class following the methods defined by Foody [36] and Congalton and Green [37].

To assess the accuracy of the cropland conversions, during the study period we selected 300 pixels representing conversion and another 300 pixels representing unchanged areas for each pattern in which the unchanged pixels were selected for the probability that they were breaking points. For each pixel, we visually inspected all 21 composite images and used high-spatial-resolution Google Earth imagery for further manual interpretation of land cover. We thus determined and recorded whether and when (occurrence year) cropland conversion occurred at these pixels; if multiple changes occurred within a single pixel, only the greatest change was used in the accuracy assessment.

3. Results

3.1. Historical Change Process of Conversion Patterns

The disturbance map (Figure 6) was rendered as a gradient according to the occurrence years to present the spatial and temporal distribution of conversion to lake during 1998–2018. The conversion was widely dispersed but most prevalent in four regions: Datong Lake, West Dongting Lake, South Dongting Lake, and East Dongting Lake (Figure 6). Overall, 447.48 km^2 of cropland was converted to lake from 1998–2018 (Table 2). Annual change peaked in 1998 due to the CFTL project's initiation, after which conversion generally declined until 2012, when it began to increase again due to new policies aimed at improving the protection and restoration of Dongting Lake.
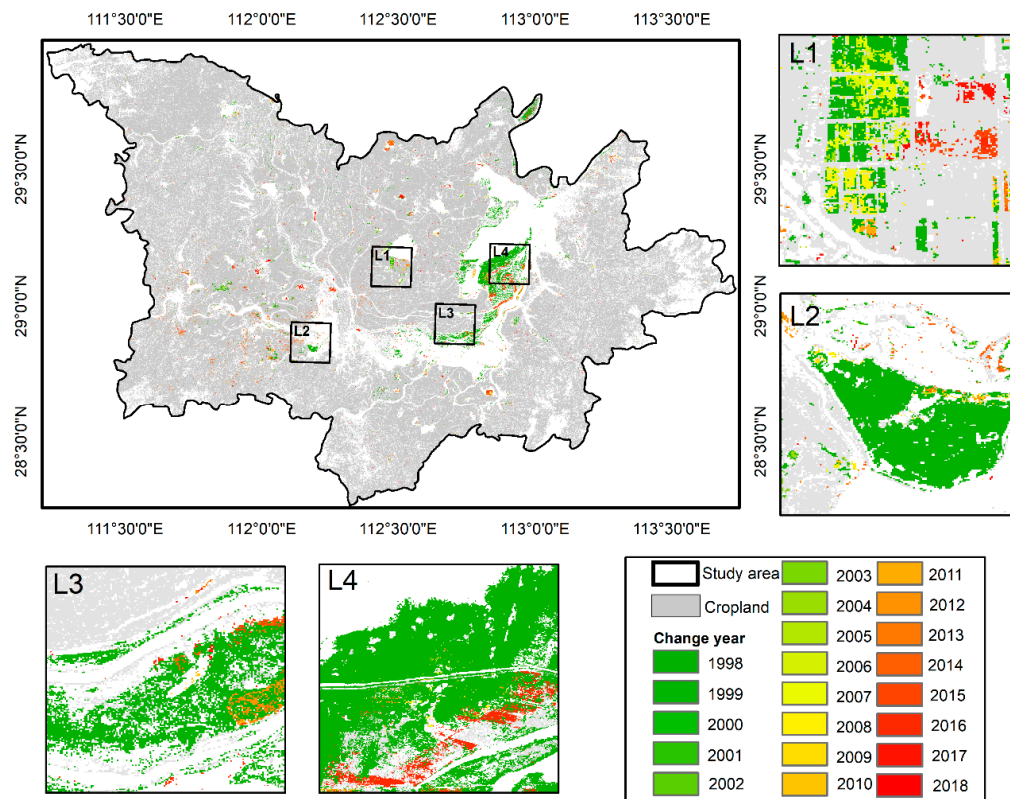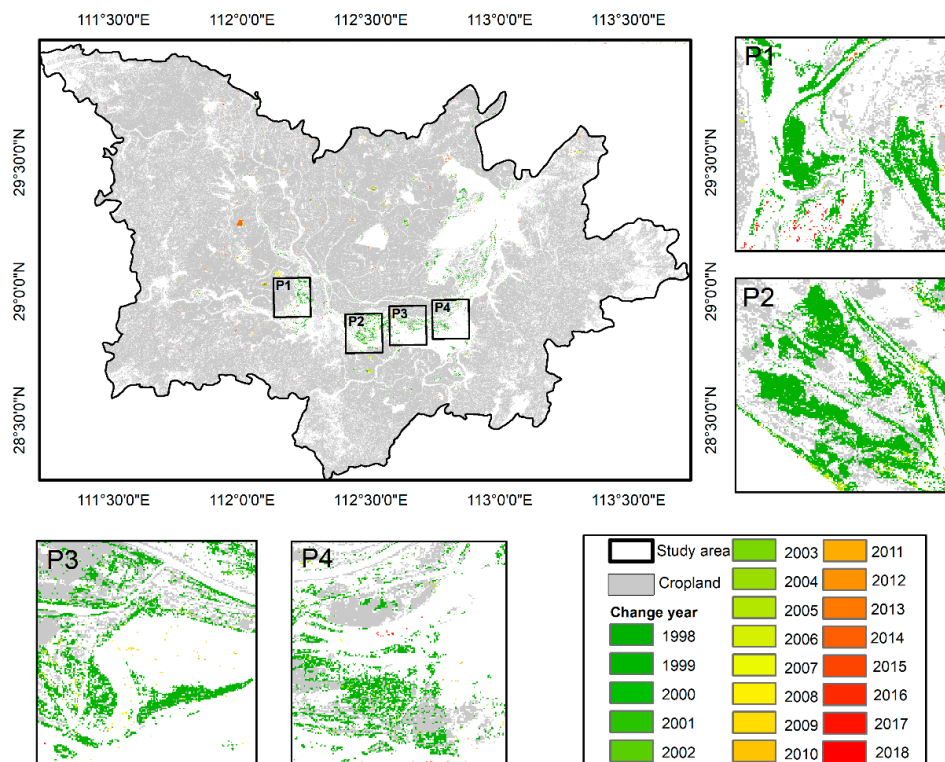
Figure 6. Year of conversion from cropland to lake with four areas shown in detail: (**L1**) Datong Lake; (**L2**) West Dongting Lake; (**L3**) South Dongting Lake; (**L4**) East Dongting Lake (scale of the four areas is 1:130,000).

Table 2. Yearly change area for both conversions from 1998 to 2018 by area and the conversion area per year as a percentage of the total converted area for all years.

| Year	Conversion to Lake		Conversion to Poplar Cultivation	
	Area (km^2)	Percentage	Area (km^2)	Percentage
1998	258.98	58.21%	221.88	44.39%
1999	3.08	0.68%	4.73	0.95%
2000	0.82	0.19%	8.67	1.73%
2001	1.13	0.28%	9.54	1.91%
2002	3.55	0.87%	4.03	0.81%
2003	5.52	1.24%	6.32	1.26%
2004	2.49	0.54%	22.19	4.44%
2005	0.91	0.21%	23.03	4.61%
2006	1.26	0.30%	7.37	1.47%
2007	3.75	0.84%	13.24	2.65%
2008	5.93	1.33%	6.50	1.30%
2009	2.42	0.52%	7.38	1.48%
2010	5.12	1.10%	7.94	1.59%
2011	2.91	0.62%	19.53	3.91%
2012	14.37	3.31%	8.02	1.61%
2013	8.25	1.80%	39.00	7.80%
2014	51.38	11.07%	34.58	6.92%
2015	13.83	3.13%	7.77	1.55%
2016	31.76	6.76%	9.01	1.80%
2017	14.62	3.47%	19.97	4.00%
2018	15.40	3.52%	19.19	3.84%
Total	447.48	100%	499.90	100%

Figure 7 was also rendered as a gradient according to the occurrence years to present the spatial and temporal distribution of poplar cultivation. Conversion to poplar cultivation was particularly prominent in West and North Dongting Lake (P1, and P2, P3, P4 in Figure 7). The patterns of poplar cultivation events in inner lakes around Datong Lake did not follow the disturbance trends of the outer West and North Dongting Lake. The total area of poplar conversion was ~12% larger than that of lake conversion over the past 21 years (Table 2). Annual conversion spiked in two periods, 2004–2005 with disturbance rates which amounted to 4.44% and 4.61%, and 2013–2014 with disturbances rates which amounted to 7.80% and 6.92%.

Figure 7. Year of conversion from cropland to poplar cultivation with four areas shown in detail: (**P1**) West Dongting Lake; (**P2**); (**P3**); (**P4**) portions of North Dongting Lake (scale of the four areas is 1:130,000).

3.2. Characterization of Two Conversion Patterns

NDVI spectral–temporal characteristics discriminated between two cropland change patterns (Figure 8). Of the pixels in which cropland was converted to lake, 82.4% showed a decline in NDVI value between 0.70–0.90. The area near Datong Lake experienced a similar decline in NDVI between 0.77–0.88 (Figure 8a), with even higher NDVI declines (0.99–1.10) during flooding events in East Dongting Lake. The average duration of conversion to lake was 2.71 years; nearly 89.9% of relevant pixels ranged from 1–5 years while 52.1% were very short (two years or less) (Figure 8b). Moreover, East Dongting Lake was dominated by one-year durations [27]. For every change pixel of conversion to poplar cultivation, we analyzed magnitude and duration characteristics of the poplar growth process for the second half of each LandTrendr trajectory. 75.6% of the relevant pixels showed an increase in NDVI value between 0.73–1.02. Higher NDVI increases clustered at the centralized poplar cultivation areas in North and West Dongting Lake (Figure 8c). The average duration of conversion to poplar cultivation was 3.17 years, while the most common durations were 1 (23.5%) and 21 (17.1%) years. Generally, longer change durations occurred in North Dongting Lake (Figure 8d) where the humid climate was suitable for poplar growth [27].
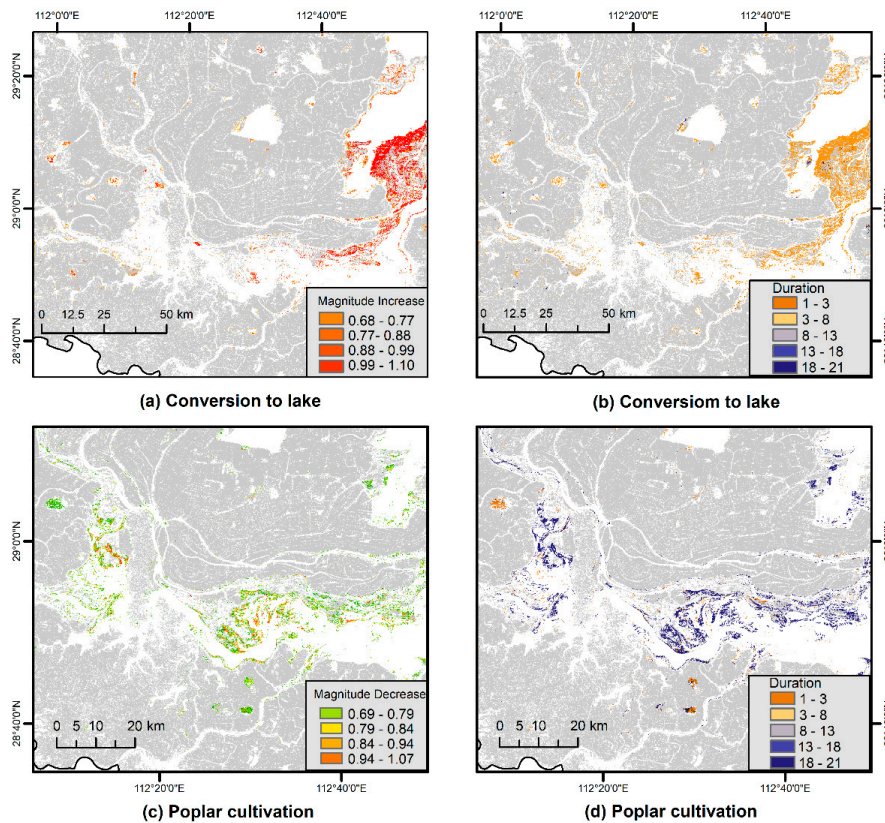
Figure 8. Magnitude and duration of conversion from cropland to (**a,b**) lake and (**c,d**) poplar cultivation in the Dongting Lake region. Close up looks for the prevalent regions of two patterns are displayed.

3.3. Accuracy Assessment

3.3.1. Accuracy Assessment for Initial Classification

The confusion matrix for the initially classified 1997 imagery (Table 3) indicated that the overall accuracy, user accuracy, and producer accuracy for each land-cover class were mostly >80%. Three categories (cropland, forest, and shoal) were most frequently misclassified. Cropland and forests were difficult to distinguish between at the 30 m Landsat resolution, because forests are often small and scattered in the study area. In addition, forests and shoals were often misclassified likely because other vegetation growing in shoals resemble forest in their spectral characteristics. Although the lower producer accuracies are indicative of errors related to the classification algorithm, the overall accuracy was greater than 85% for each classification period, indicating the RF classifier was sufficient for this study area.

Table 3. Confusion matrix for the 1997 classified imagery.

	Validation Data					
Class	**Water**	**Cropland**	**Forest**	**Urban**	**Shoal**	**User Accuracy**
Water	179	0	0	0	0	100%
Cropland	1	153	24	10	30	70.2%
Forest	0	14	153	1	17	82.7%
Urban	0	3	1	168	1	97.1%
Shoal	0	10	2	1	132	91.0%
Total	180	180	180	180	180	
Producer Accuracy	99.4%	85.0%	85.0%	93.3%	73.3%	

Overall accuracy = 87.2%.

3.3.2. Accuracy Assessment for LandTrendr

The results of the segmentation and fitting algorithms suggest that both conversion patterns were successfully captured by LandTrendr. Both accuracy assessments (Table 4) indicated high producer and user accuracies, with the overall accuracy of conversion to lake (87.0%) being slightly higher than conversion to poplar cultivation (83.8%). One typical area of each conversion type (Qingshan polder and Jicheng polder described in Figure 2) was further studied to validate the algorithm, RF classification (Figure 9a2,b2) in specific years finished to help us better analyze the relevant changes. In the first area (Figure 9a), original cropland was abandoned after the CFTL and converted to lake from 1998 onward, a change conducive to wetland ecological recovery [28]. In the second area (Figure 9b), cropland was abandoned before poplar planting prior to 2002 but these plantings were decreasing by 2010.
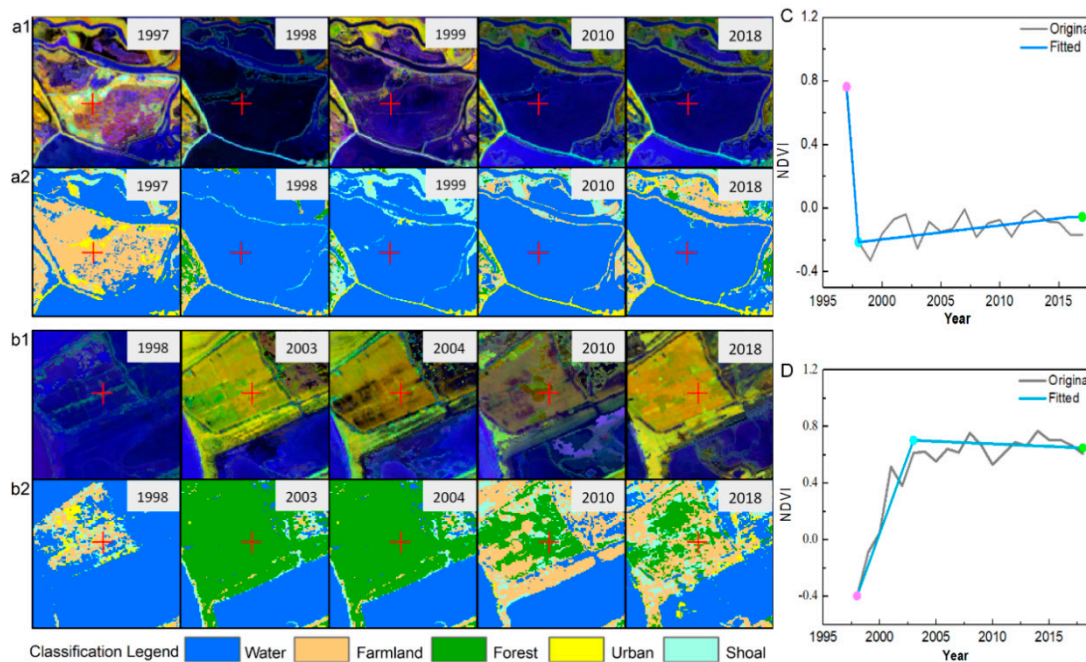
Figure 9. Landsat spectral trajectories and LandTrendr fitted trajectories in typical areas (crosses indicate trajectory locations) for (**a,C**) conversion to lake and (**b,D**) conversion to poplar cultivation. Related imagery (a1,b1,bands 4–5–3) and corresponding Landsat classification results(a2,b2) are also shown at left.

Table 4. Accuracy assessments for change detection in both conversion patterns.

|	Changed Pixels	Stable Pixels	Total	User Accuracy
Conversion to Lake				
Changed pixels	258	42	300	86.0%
Stable pixels	36	264	300	88.0%
Total	294	306		
Producer Accuracy	87.8	86.3%	Overall	87.0%
Conversion to Poplar Cultivation				
	Changed Pixels	Stable Pixels	Total	User Accuracy
Changed pixels	245	55	300	81.7%
Stable pixels	42	258	300	86.0%
Total	287	313		
Producer Accuracy	85.4%	82.4%	Overall	83.8%

Note: Stable pixels means areas where land cover was persistent throughout the time of the analysis (1998–2018).

4. Discussion

4.1. Mapping Approach

LandTrendr in this study detected different spatial distribution characteristics accurately under both conversion patterns. Conversion to lake detected most prevalent around Datong Lake, because of the Government encouraged the improvement of water storage capacity of the inner lake by excavating deep ponds near Datong Lake (L1 in Figure 6), while the East, South, and West Dongting Lake areas (L2, L3, and L4 in Figure 6 respectively) have also undergone large-scale improvements to improve their interconnectivity and improve the ecological function of Dongting Lake as a whole [38]. Conversion to poplar cultivation was particularly prominent in West and North Dongting Lake due to raw material supply bases set up in this regions to develop the local economy, resulting in large-scale poplar planting in this district.

Using LandTrendr resulted in producer and user accuracies high enough to detecting different spatial and temporal characteristics under both conversion patterns. Compare the user's accuracy between changed and stable pixels, the relatively low accuracy for changed pixels indicated that commission errors did occur; we identified four types (Figure 10). First, errors can be caused by transient change events like floods (such as the major flooding in 1998), which can lead to incorrect classification as conversion to lake (Figure 10a). Second, non-abrupt conversion to lake, which occurs when the NDVI signals are unstable, leads to advance or lag segments in the fitted trajectories (Figure 10b). Third, reed plantings have the same NDVI fluctuation range as poplars and the two can be difficult to distinguish (Figure 10c). Fourth, non-abrupt poplar cultivation events produce gradual changes while the NDVI before or after the conversion have strong fluctuations (Figure 10d). In these cases, the fitted trajectory does not reach the set p-value parameter (0.05), making the segmentation of the LandTrendr return a straight line as a segment for whole trajectory. Despite these potential errors, the high producer and user accuracies for both conversion patterns imply that the LandTrendr approach used in this research was robust.
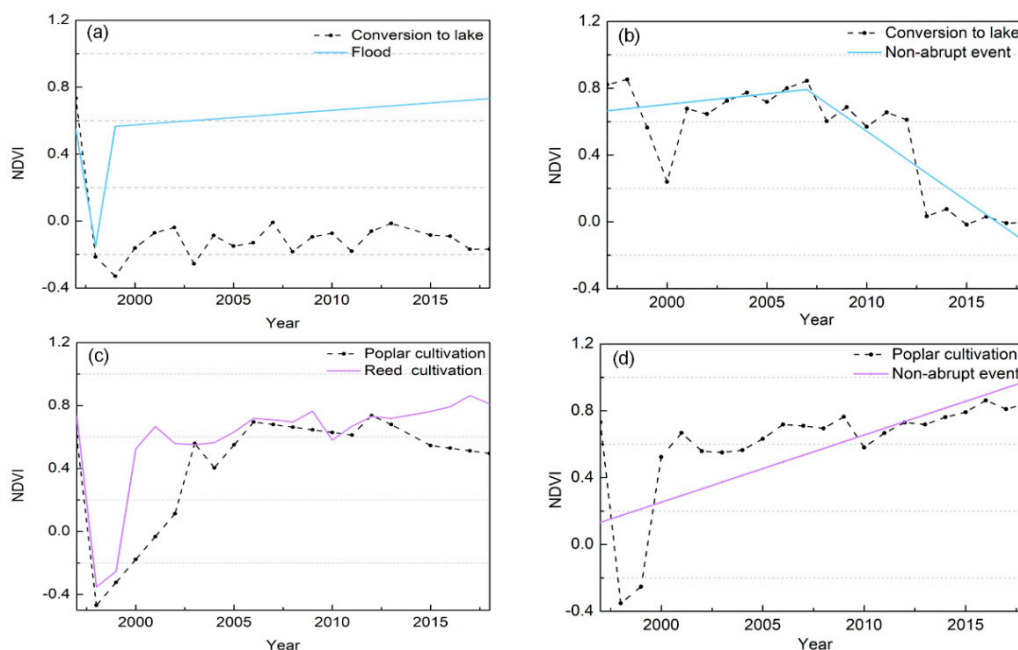
Figure 10. Four types of commission errors possible when assessing cropland conversion with LandTrendr: (**a**) transient floods misclassified as conversion to lake; (**b**) non-abrupt conversion to lake; (**c**) reed cultivation producing a similar NDVI signal as poplar cultivation; (**d**) non-abrupt poplar cultivation. The typical trajectory for each error (blue or purple solid line) and real cropland conversion (black dotted line) were extracted from NDVI series.

4.2. Benefits of Change Detection Using LandTrendr in GEE

Accurate information about the timing and extent of cropland change is crucial for environmental assessment and policy making [39]. In contrast to analyzed cropland abandonment and re-cultivation via LandTrendr [40], we used this approach to study cropland conversion to other land cover classes. By using this temporal segmentation algorithm with a time series of Landsat data, we were able to map the spatial and temporal characteristics of different cropland conversion type. One clear advantage of Landsat is the availability of consistent data for over three decades, allowing long-term analyses. Compared to multi-date change mapping, the Landsat time series used here allowed us to map more deviations in detail [41].

Although change detection-related studies have seen a considerable amount of research using LandTrendr using data on local servers [25,35,42], the algorithm is still limited by time-consuming data management work. In contrast, there are a few advantages of LandTrendr with GEE support to monitor cropland change. Firstly, images are mostly prepared and updated by Google for cropland change analysis. Secondly, GEE had an increased speed and great advantages in terms of vast data handling and management cost [43,44], after data processing, the actual LandTrendr computational cost and time are also reduced. Moreover, implementation in GEE makes it available to a much broader base of users for those lack the technical capacity, experience, or financial means.

4.3. Research Limitations

Vegetation indices have been regarded as better variables than individual spectral bands, in terms of monitoring land cover change, because they can reduce the impacts of external factors such as topography and atmosphere on the surface reflectance. Selecting suitable vegetation indices is critical for successfully detecting cropland conversion in our study; different vegetation indices, such as Enhanced Vegetation Index (EVI) [20] and NDVI [32,45], have been used for this purpose. Research shows that NDVI distinguishes cropland change better than other indices [46,47], but there are still some limitations to applying the LandTrendr algorithm with NDVI. One example is the disturbance caused by other vegetation, such as the reeds in our study region that produced an NDVI signal similar to poplar and thus influenced the detection result. It is unclear whether or not NDVI is the best index to use for the Dongting Lake region; more research is needed to identify an optimum.

5. Conclusions

In this study, we showed the effectiveness of a trajectory-based change detection approach to characterize two cropland change patterns in China's Dongting Lake region. By using the LandTrendr algorithm with Landsat imagery derived from the Google Earth Engine, we detected and mapped the conversion of cropland to lake and poplar cultivation with overall accuracies of 87.0% and 83.8%, respectively. Conversion to lake covered a wider range, mainly distributed in areas surrounding the outer lake and Datong Lake, while conversion to poplar cultivation was more prevalent in North and West Dongting Lake. Over the entire study period, almost 947.38 km^2 of cropland was converted, with poplar accounting for 52.42 km^2 more than lake. Some differences were apparent between the two conversion patterns when their spectral–temporal characteristics were compared. For lake conversion pixels, 82.4% had a decline in NDVI value between 0.70–0.90, while 75.6% of poplar-conversion pixels increased by 0.73–1.02. We also found a high proportion of short-duration (two years or less) pixels for conversion to lake, while the average duration of poplar cultivation pixels was a bit longer. These results can assist researchers and managers in better understanding the conversion processes over time in this region while providing baseline information for assessing the environmental influences of cropland conversion in the Dongting Lake region.

Author Contributions: Conceptualization, X.L. and L.Z.; Data curation, L.Z., L.W. and Y.T.; Formal analysis, L.Z., L.W. and Y.T.; Methodology, L.Z. and Y.T.; Supervision, X.L.; Validation, and L.W.; Visualization, Y.M.; Writing—Original Draft Preparation, L.Z.; Writing—Review & Editing, X.L., L.W. and Y.M.

Conflicts of Interest: The authors declare no conflict of interest.

References

1. Xu, C.; Mcgowan, S.; Lei, X.; Zeng, L.; Yang, X. Effects of hydrological regulation and anthropogenic pollutants on Dongting Lake in the Yangtze floodplain. *Ecohydrology* **2016**, *9*, 315–325.

2. Hereher, M.E. Environmental monitoring and change assessment of Toshka lakes in southern Egypt using remote sensing. *Environ. Earth Sci.* **2015**, *73*, 3623–3632. [CrossRef]

3. Qi, S.H.; Brown, D.G.; Tian, Q.; Jiang, L.G.; Zhao, T.T.; Bergen, K.M. Inundation extent and flood frequency mapping using LANDSAT imagery and digital elevation models. *Mapp. Sci. Remote Sens.* **2009**, *46*, 101–127. [CrossRef]

4. Kraemer, R.; Prishchepov, A.V.; Müller, D.; Kuemmerle, T.; Radeloff, V.C.; Dara, A.; Terekhov, A.; Frühauf, M. Long-term agricultural land-cover change and potential for cropland expansion in the former Virgin Lands area of Kazakhstan. *Environ. Res. Lett.* **2015**, *10*, 054012. [CrossRef]

5. Woodcock, C.E.; Richard, A.; Martha, A.; Alan, B.; Robert, B.; Warren, C.; Feng, G.; Goward, S.N.; Dennis, H.; Eileen, H. Free access to Landsat imagery. *Science* **2008**, *320*, 1011. [CrossRef] [PubMed]

6. Röder, A.; Stellmes, M.; Hill, J.; Kuemmerle, T.; Tsiourlis, G.M. Analysing land cover change using time series analysis of Landsat data and geoinformation processing. A natural experiment in Northern Greece. *Proc. SPIE Int. Soc. Opt. Eng.* **2008**, *7104*, 43–56.

7. Rogan, J.; Franklin, J.; Roberts, D.A. A comparison of methods for monitoring multitemporal vegetation change using Thematic Mapper imagery. *Remote Sens. Environ.* **2002**, *80*, 143–156. [CrossRef]

8. Wohlfart, C.; Mack, B.; Liu, G.; Kuenzer, C. Multi-faceted land cover and land use change analyses in the Yellow River Basin based on dense Landsat time series: Exemplary analysis in mining, agriculture, forest, and urban areas. *Appl. Geogr.* **2017**, *85*, 73–88. [CrossRef]

9. Liao, C.; Feng, Z.; Peng, L.I.; Zhang, J. Monitoring the spatio-temporal dynamics of swidden agriculture and fallow vegetation recovery using Landsat imagery in northern Laos. *Acta Geogr. Sin.* **2015**, *25*, 1218–1234. [CrossRef]

10. Forkuor, G.; Conrad, C.; Thiel, M.; Zoungrana, B.; Tondoh, J. Multiscale Remote Sensing to Map the Spatial Distribution and Extent of Cropland in the Sudanian Savanna of West Africa. *Remote Sens.* **2017**, *9*, 839. [CrossRef]

11. Falkowski, M.J.; Manning, J.A. Parcel-based classification of agricultural crops via multitemporal Landsat imagery for monitoring habitat availability of western burrowing owls in the Imperial Valley agro-ecosystem. *Can. J. Remote Sens.* **2010**, *36*, 750–762. [CrossRef]

12. Justice, C.J. Landsat-derived cropland mask for Tanzania using 2010–2013 time series and decision tree classifier methods. In Proceedings of the Agu Fall Meeting, College Park, MD, USA, 17 December 2015.

13. Xu, Y.; Yu, L.; Zhao, F.R.; Cai, X.; Zhao, J.; Lu, H.; Gong, P. Tracking annual cropland changes from 1984 to 2016 using time-series Landsat images with a change-detection and post-classification approach: Experiments from three sites in Africa. *Remote Sens. Environ.* **2018**, *218*, 13–31. [CrossRef]

14. Zhe, Z. Change detection using landsat time series: A review of frequencies, preprocessing, algorithms, and applications. *Isprs J. Photogramm. Remote Sens.* **2017**, *130*, 370–384. [CrossRef]

15. Lu, D.; Li, G.; Moran, E. Current situation and needs of change detection techniques. *Int. J. Image Data Fusion* **2014**, *5*, 13–38. [CrossRef]

16. Griffiths, P.; Kuemmerle, T.; Kennedy, R.E.; Abrudan, I.V.; Knorn, J.; Hostert, P. Using annual time-series of Landsat images to assess the effects of forest restitution in post-socialist Romania. *Remote Sens. Environ.* **2012**, *118*, 199–214. [CrossRef]

17. Novo-Fernández, A.; Franks, S.; Wehenkel, C.; López-Serrano, P.M.; Molinier, M.; López-Sánchez, C.A. Landsat time series analysis for temperate forest cover change detection in the Sierra Madre Occidental, Durango, Mexico. *Int. J. Appl. Earth Obs. Geoinf.* **2018**, *73*, 230–244. [CrossRef]

18. Verbesselt, J.; Herold, M.; Hyndman, R.; Zeileis, A.; Culvenor, D. A robust approach for phenological change detection within satellite image time series. In Proceedings of the Analysis of Multi-Temporal Remote Sensing Images, Trento, Italy, 12–14 July 2011.

19. Fatikhunnada, A.; Seminar, K.B.; Solahudin, M.; Buono, A. Optimization of Parallel K-means for Java Paddy Mapping Using Time-series Satellite Imagery. *Telkomnika* **2018**, *16*, 1409–1415. [CrossRef]

20. Huang, K.; Tao, Z.; Xiang, Z. Extreme Drought-induced Trend Changes in MODIS EVI Time Series in Yunnan, China. *IOP Conf. Ser. Earth Environ. Sci.* **2014**, *17*, 012070. [CrossRef]

21. Schneibel, A.; Stellmes, M.; Röder, A.; Frantz, D.; Kowalski, B.; Haß, E.; Hill, J. Assessment of spatio-temporal changes of smallholder cultivation patterns in the Angolan Miombo belt using segmentation of Landsat time series. *Remote Sens. Environ.* **2017**, *195*, 118–129. [CrossRef]

22. Dara, A.; Baumann, M.; Kuemmerle, T.; Pflugmacher, D.; Rabe, A.; Griffiths, P.; Hölzel, N.; Kamp, J.; Freitag, M.; Hostert, P. Mapping the timing of cropland abandonment and recultivation in northern Kazakhstan using annual Landsat time series. *Remote Sens. Environ.* **2018**, *213*, 49–60. [CrossRef]

23. Zhe, Z.; Woodcock, C.E. Continuous change detection and classification of land cover using all available Landsat data. *Remote Sens. Environ.* **2014**, *144*, 152–171. [CrossRef]

24. Gorelick, N.; Hancher, M.; Dixon, M.; Ilyushchenko, S.; Thau, D.; Moore, R. Google Earth Engine: Planetary-scale geospatial analysis for everyone. *Remote Sens. Environ.* **2017**, *202*, 18–27. [CrossRef]

25. Watts, L.M.; Laffan, S.W. Effectiveness of the BFAST algorithm for detecting vegetation response patterns in a semi-arid region. *Remote Sens. Environ.* **2014**, *154*, 234–245. [CrossRef]

26. Li, Z.; Wu, W.; Liu, X.; Fath, B.D.; Sun, H.; Liu, X.; Xiao, X.; Cao, J. Land use/cover change and regional climate change in an arid grassland ecosystem of Inner Mongolia, China. *Ecol. Model.* **2017**, *353*, 86–94. [CrossRef]

27. Shelestov, A.; Lavreniuk, M.; Kussul, N.; Novikov, A.; Skakun, S. Exploring Google Earth Engine Platform for Big Data Processing: Classification of Multi-Temporal Satellite Imagery for Crop Mapping. *Front. Earth Sci.* **2017**, *5*, 17. [CrossRef]

28. Hu, Y.; Huang, J.; Yun, D.; Han, P.; Wei, H. Monitoring Spatial and Temporal Dynamics of Flood Regimes and Their Relation to Wetland Landscape Patterns in Dongting Lake from MODIS Time-Series Imagery. *Remote Sens.* **2015**, *7*, 7494–7520. [CrossRef]

29. Li, Y.; Chen, X.; Xie, Y.; Li, X.; Li, F.; Hou, Z. Effects of young poplar plantations on understory plant diversity in the Dongting Lake wetlands, China. *Sci. Rep.* **2014**, *4*, 6339. [CrossRef]

30. Roy, D.P.; Kovalskyy, V.; Zhang, H.K.; Vermote, E.F.; Yan, L.; Kumar, S.S.; Egorov, A. Characterization of Landsat-7 to Landsat-8 reflective wavelength and normalized difference vegetation index continuity. *Remote Sens. Environ.* **2016**, *185*, 57–70. [CrossRef]

31. Simonetti, D.; Simonetti, E.; Szantoi, Z.; Lupi, A.; Eva, H.D. First Results From the Phenology-Based Synthesis Classifier Using Landsat 8 Imagery. *IEEE Geosci. Remote Sens. Lett.* **2015**, *12*, 1496–1500. [CrossRef]

32. Zhang, Y.; Gao, J.; Liu, L.; Wang, Z.; Ding, M.; Yang, X. NDVI-based vegetation changes and their responses to climate change from 1982 to 2011: A case study in the Koshi River Basin in the middle Himalayas. *Glob. Planet. Chang.* **2013**, *108*, 139–148. [CrossRef]

33. Bai, J.J.; Bai, J.T.; Wang, L. Spatio-temporal Change of Vegetation NDVI and Its Relations with Regional Climate in Northern Shaanxi Province in 2000–2010. *Sci. Geogr. Sin.* **2014**, *34*, 882–888.

34. Mainknorn, M.; Cohen, W.B.; Kennedy, R.E.; Grodzki, W.; Pflugmacher, D.; Griffiths, P.; Hostert, P. Monitoring coniferous forest biomass change using a Landsat trajectory-based approach. *Remote Sens. Environ.* **2013**, *139*, 277–290. [CrossRef]

35. Kennedy, R.E.; Yang, Z.; Cohen, W.B. Detecting trends in forest disturbance and recovery using yearly Landsat time series: 1. LandTrendr—Temporal segmentation algorithms. *Remote Sens. Environ.* **2010**, *114*, 2897–2910. [CrossRef]

36. Foody, G.M. Status of land cover classification accuracy assessment. *Remote Sens. Environ.* **2002**, *80*, 185–201. [CrossRef]

37. Congalton, R.G.; Green, K. Practical look at the sources of confusion in error matrix generation. *Photogramm. Eng. Remote Sens.* **1993**, *59*, 641–644.

38. Bo, Y.; Zeng, F.; Yuan, M.; Li, D.; Qiu, Y.; Li, J. Measurement of Dongting Lake Area Based on Visual Interpretation of Polders. *Proced. Environ. Sci.* **2011**, *10*, 2684–2689.

39. Zhang, P.L.; Bo, L.R.; Chao, J. An Object-based Basic Farmland Change Detection Using High Spatial Resolution Image and GIS Data of Land Use Planning. *Key Eng. Mater.* **2012**, *500*, 492–499. [CrossRef]

40. Yin, H.; Prishchepov, A.V.; Kuemmerle, T.; Bleyhl, B.; Buchner, J.; Radeloff, V.C. Mapping agricultural land abandonment from spatial and temporal segmentation of Landsat time series. *Remote Sens. Environ.* **2018**, *210*, 12–24. [CrossRef]

41. Schmidt, M.; Pringle, M.; Devadas, R.; Denham, R.; Dan, T. A Framework for Large-Area Mapping of Past and Present Cropping Activity Using Seasonal Landsat Images and Time Series Metrics. *Remote Sens.* **2016**, *8*, 312. [CrossRef]

42. Schwantes, A.M.; Swenson, J.J.; Jackson, R.B. Quantifying drought-induced tree mortality in the open canopy woodlands of central Texas. *Remote Sens. Environ.* **2016**, *181*, 54–64. [CrossRef]

43. Long, T.; Zhang, Z.; He, G.; Jiao, W.; Tang, C.; Wu, B.; Zhang, X.; Wang, G.; Yin, R. 30 m resolution Global Annual Burned Area Mapping based on Landsat images and Google Earth Engine. *Remote Sens.* **2019**, *11*, 489. [CrossRef]

44. Dong, J.; Xiao, X.; Menarguez, M.A.; Zhang, G.; Qin, Y.; Thau, D.; Biradar, C.; Iii, B.M. Mapping paddy rice planting area in northeastern Asia with Landsat 8 images, phenology-based algorithm and Google Earth Engine. *Remote Sens. Environ.* **2016**, *185*, 142–154. [CrossRef] [PubMed]

45. Shrestha, R.; Di, L.; Yu, E.G.; Kang, L.; Shao, Y.Z.; Bai, Y.Q. Regression model to estimate flood impact on corn yield using MODIS NDVI and USDA cropland data layer. *J. Integr. Agric.* **2017**, *16*, 398–407. [CrossRef]

46. Tian, H.; Wu, M.; Wang, L.; Niu, Z. Mapping Early, Middle and Late Rice Extent Using Sentinel-1A and Landsat-8 Data in the Poyang Lake Plain, China. *Sensors* **2018**, *18*, 185. [CrossRef]

47. Tong, X.; Brandt, M.; Hiernaux, P.; Herrmann, S.M.; Feng, T.; Prishchepov, A.V.; Fensholt, R. Revisiting the coupling between NDVI trends and cropland changes in the Sahel drylands: A case study in western Niger. *Remote Sens. Environ.* **2017**, *191*, 286–296. [CrossRef]